Computational and Theoretical Chemistry 1031 (2014) 1–6

Contents lists available at ScienceDirect

Computational and Theoretical Chemistry

journal homepage: www.elsevier.com/locate/comptc

A theoretical investigation of the α-MnO_2 (1 1 0) surface

Yue Liu, Lin Yu *, Ming Sun, Guiqiang Diao, Bang Lan, Gao Cheng

School of Chemical Engineering and Light Industry, Guangdong University of Technology, Guangzhou 510006, PR China

ARTICLE INFO

Article history:
Received 2 November 2013
Received in revised form 4 January 2014
Accepted 4 January 2014
Available online 11 January 2014

Keywords:
α-MnO_2 surface
Density functional theory
Surface energy
Magnetic property

ABSTRACT

Density functional theory calculations have been carried out to investigate the α-MnO_2 (1 1 0) surface. It is shown that the energies of nonmagnetic (NM) and ferromagnetic (FM) states are higher than that of the antiferromagnetic (AFM) states, and at the same time some AFM states have similar stabilities. Using a 27-layer thick periodically repeated slab model, the (1 1 0) surface with all kinds of no reconstruction terminations have been calculated. The AFM surface T1 with the lowest surface energy of 0.77 J m^{-2} is the most stable surface, which exposes the crystal 2 × 2 semitunnel to air. When we put OH^- ions onto the surface T1, our computed results agree with the experimental atomic force microscopy results. We hope that our calculations would be helpful for the understanding of the α-MnO_2 (1 1 0) surface and further exploration of some adsorptions and reactions on it.

1. Introduction

α-MnO_2 can act as an efficient and robust water oxidation catalyst under visible light in strong acidic conditions [1], and O_2 reduction catalyst in a KOH solution [2]. Based on our experiments of dimethyl ether combustion, MnO_2 catalytic activities are mainly dominated by the crystalline phase, and α-MnO_2 is better than γ-MnO_2 and β-MnO_2 [3]. The α-MnO_2 crystal structures can be found from XRD pattern (JCPDS 44-0141) and the recent reports [4,5]. In terms of magnetism, the ground state of α-MnO_2 is considered to be antiferromagnetic or helical magnetic [6,7]. Using atomic force microscopy (AFM), Yamamoto et al. determined the atomic configuration and topography of the α-MnO_2 surface [8].

Computational chemistry and molecular modelling tools are capable of simulating crystal and surface structures and advancing our understanding of adsorption and catalysis behaviors on solid surfaces. In 2007, Franchini et al. reported the structural, electronic, magnetic, and thermodynamical properties of MnO, Mn_3O_4, α-Mn_2O_3, and β-MnO_2 crystals by density functional theory (DFT) methods [9]; in 2008, Kwon et al. reported the calculations of layered δ-MnO_2 [10]; in 2011, Oxford and Chaka reported the calculations of many kinds of β-MnO_2 surfaces [11]. For α-MnO_2 crystal, Cockayne and Li calculated the atomic, electronic, and magnetic properties in 2012 [12]; Duan et al. calculated Ni/Co/Fe-doped α-MnO_2 in 2012 and 2013 [13,14]. For α-MnO_2 surface, Tang et al. used the oxygen-rich and oxygen-lean α-MnO_2 surface model to explain the surface structure sensitivity of manganese oxides for low-temperature selective catalytic reduction of NO with NH_3 in 2011 and 2012 [15,16].

To achieve a deeper understanding of the α-MnO_2 crystal and surface, DFT with periodic boundary conditions have been applied to calculate α-MnO_2 crystal structures with different magnetic arrangements and different kinds of α-MnO_2 (1 1 0) surface terminations. The next section gives details of the computational model and the parameters used. The results section examines the crystal and surface structures. Then the most favorable crystal and surface structures are confirmed.

2. Computational method

The calculations were performed with DFT with periodic boundary conditions [11]. The exchange–correlation interaction was treated within the generalized gradient approximation (GGA) with the functional parameterized by Perdew, Burke and Enzerhof (PBE) [17]. Atomic basis sets were applied numerically in terms of a double numerical plus polarization function [18] and a global orbital cutoff of 4.7 Å was employed. The geometry optimization convergence tolerances of the energy, gradient, and displacement were 10^{-5} Hartree, 2×10^{-3} Hartree $Å^{-1}$, and 5×10^{-3} Å, respectively. All the structures were optimized at the same level of theory unless otherwise mentioned. The surface energy γ (J m^{-2}) is used to estimate the surface stability as follows:

$$\gamma = (U_{surf} - U_{bulk})/S_{surf} \quad (1)$$

where U_{surf} and U_{bulk} are the energies of the surface and crystal with the same number of bulk ions, respectively, and S_{surf} is the surface area. It is necessary to ensure that a sufficient number

* Corresponding author. Tel.: +86 20 39322202; fax: +86 20 39322231.
E-mail address: gych@gdut.edu.cn (L. Yu).

2210-271X/$ - see front matter © 2014 Elsevier B.V. All rights reserved.
http://dx.doi.org/10.1016/j.comptc.2014.01.003

of layers are modelled so that the energy of the bulk has converged.

Although using effective on-site coulomb value (U) and exchange value (J) such as in Ref. [19] or some hybrid functionals such as in Ref. [9] may make some calculations fit to the experimental results. However, based on the computations of Franchini et al. [9], hybrid functionals and DFT + U tend to favor oxygen-poor compounds, leading to incorrect trends in calculated relative formation energies for various manganese oxides. Oxford et al. [11] also reported that the structures and energies would be better agreement with experimental results when the U correction was not included during the calculations of β-MnO_2 surfaces. By comparing our computational results of α-MnO_2 crystal (without using U and J) with the results from Cockayne et al. [12] (using U and J) in Section 3.1, we also find that our structure results are more near the experimental results such as in JCPDS 44-0141. Therefore, we did not include the U and J parameters in our DFT calculations. In addition, there was no uniformed U for MnO_2. Liechtenstein et al. [19] suggested U to be 2.8 eV for β-MnO_2. Franchini et al. [7] also tested different U such as 3 eV, 4 eV and 6 eV to get that 4 eV was better than the others, while the structure and energy results of 4 eV were not better than that of without using U in their Figs. 2 and 5, respectively for β-MnO_2. For α-MnO_2 crystals, Cockayne and Li [12] used 2.8 eV, but Duan et al. used 2.5 eV for Fe doped α-MnO_2 [13] and 2.8 eV for Co/Ni doped α-MnO_2 [14]. There would be different U and J values needed for different kinds of MnO_2 crystals and surfaces. For our system, there would be different U and J for α-MnO_2 crystal and its (1 1 0) surface. Then the surface energy γ would be no means when we used different U to calculate the energies of crystal and surface. In the present paper, all the simulations were based on the same method (without U correction), the comparison of the surface energies can provide an insight into the surface stabilities. All electron DFT calculations were performed using a DMol3 package [20–22] in Materials Studio (version 5.5).

3. Results and discussion

3.1. Calculations of α-MnO_2 crystal

Although α-MnO_2 has been shown to exhibit an antiferromagnetic or helical magnetic spin arrangement [6,7], an idealized collinear arrangement was modeled in this study, as has been done in previous studies [9,11]. An ideal α-MnO_2 supercell ($2 \times 1 \times 4$, $Mn_{32}O_{64}$) with a tetragonal structure was used to simulate the nonmagnetic (NM), ferromagnetic (FM), and four kinds of antiferromagnetic (AFM1–AFM4) states, as shown in Fig. 1 (where the O^{2-} ions are shown in red, the NM, FM and spin 'up' Mn^{4+} ions are in lavender, and the spin 'down' Mn^{4+} ions are in green). It should be noted that NM, AFM1, AFM2 and AFM4 are shown from top view in Fig. 1, and the rear Mn^{4+} ions possess the same spin state as the ions seen in the top view. AFM3 has the same top view as AFM1, but the behind Mn^{4+} ion possesses different spin state as shown in Fig. 1E. The Monkhorst–Pack k point sampling was set as $3 \times 3 \times 3$ in the supercell [23]. The optimized lattice parameters and energies are collected in Table 1.

From Table 1, we can see that the crystal energy is dramatically influenced by the magnetic arrangement. The NM and FM structures are 722.473 and 87.633 meV per formula unit higher in energy than AFM1. The AFM1 state is the ground state. It lies 3.096, 18.723 and 18.938 meV per formula unit lower than AFM2, AFM3 and AFM4 states, respectively. It should be noted that the energy difference between AFM1 and AFM2 is small, and Cockayne and Li [12] and Duan et al. [13,14] calculated α-MnO_2 and Ni/Co/Fe-doped α-MnO_2 crystal with the AFM2 state. The optimized bulk lattice constants of 9.8349 Å (−0.2%) and 2.8805 Å (+0.6%) for the AFM1 state are in excellent agreement with experimental JCPDS 44-0141 values (percent error shown in parentheses) and other experimental results [4,5]. It is clear that our structures are better than that of 9.702 Å (−1.52%) and 2.856 Å (−0.30%) from the DFT + U computations

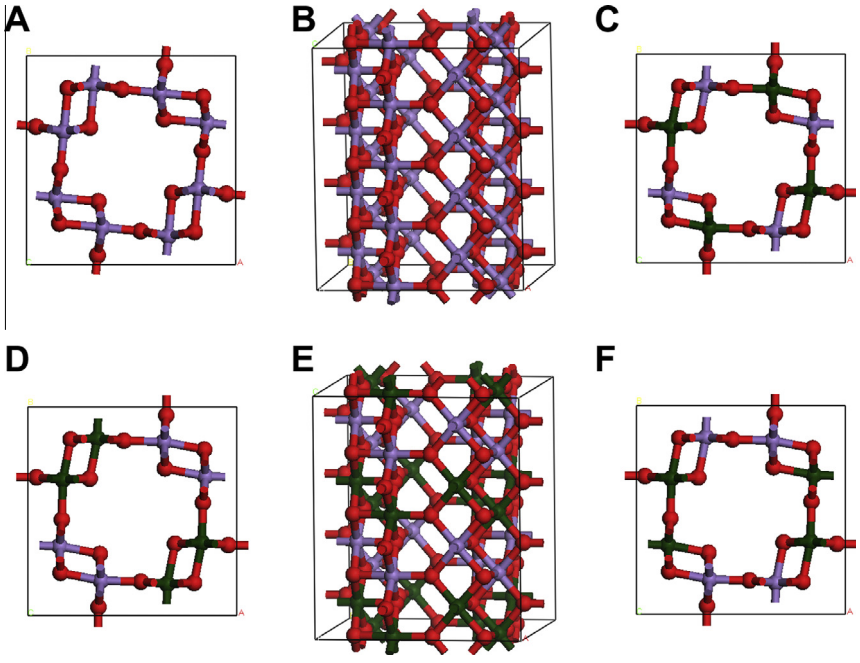

Fig. 1. The optimized α-MnO_2 crystal with the supercell $Mn_{32}O_{64}$, where the O^{2-} ions are shown in red, the NM, FM and spin 'up' Mn^{4+} ions are in lavender, and the spin 'down' Mn^{4+} ions are in green. (A) top view of NM state; (B) side view of FM state; (C) top view of AFM1 state; (D) top view of AFM2 state; (E) side view of AFM3 state; and (F) top view of AFM4 state. (For interpretation of the references to colour in this figure legend, the reader is referred to the web version of this article.)

Table 1
Comparison of the optimized lattice parameters with previous results and the relative energies of different magnetic arrangements per MnO_2 unit.

	a (Å)	b (Å)	c (Å)	A (°)	β (°)	γ (°)	Space group	Total energy
AFM1	9.8349	–	2.8805	–	–	–	*I4/m*	0[a]
AFM2	9.8062	–	2.8756	–	–	–	*I4/m*	3.096[a]
AFM3	9.8591	–	2.8750	–	–	–	*I4/m*	18.723[a]
AFM4	9.8795	–	2.8845	–	–	–	*I4/m*	18.938[a]
FM	9.8697	–	2.8822	–	–	–	*I4/m*	87.633[a]
NM	9.6505	–	2.8105	–	–	–	*I4/m*	722.473[a]
JCPDS 44-0141	9.8521	–	2.8647	–	–	–	*I4/m*	–
Ref. [4]	9.8241	–	2.856	–	–	–	*I4/m*	–
Ref. [5]	9.8394	9.790	2.856	–	90.138	–	*I2/m*	–
Ref. [12]	9.702	9.685	2.856	–	90.041	–	*I2/m*	–

[a] The relative energy is given in units of meV per MnO_2 unit.

[12]. The detailed calculated coordinates of AFM1 are listed in the Supporting materials. We will use the energy of AFM1 as U_{bulk} in Sections 3.2 and 3.3 to calculate the surface energy.

3.2. Calculations of α-MnO_2 (1 1 0) surface

3.2.1. Test different thickness and different kinds of fixing types of α-MnO_2 (1 1 0) surface

To test different thickness and different kinds of fixing types of α-MnO_2 (1 1 0) surface, numerous attempts have been made to simulate Mn_8O_{16}, $Mn_{12}O_{24}$ and $Mn_{16}O_{32}$ surfaces, with 18-layer, 27-layer and 36-layer thick periodically repeated slabs, respectively. Only in this part, we used lower calculation accuracy, i.e., the geometry optimization convergence tolerances of the energy, gradient, and displacement were 2×10^{-5} Hartree, 4×10^{-3} Hartree Å^{-1}, and 5×10^{-3} Å, respectively, and a global orbital cutoff of 4.4 Å was employed in the atomic basis sets. In fact, when we fixed only the bottom Mn^{4+} ion, other ions would fall down to the bottom and the whole structure crashed. We could get a reasonable structure with at least 10 bottom atoms fixed. On the other hand, the surface would be more like the crystal when we fixed more atoms. After many tests, we found that $Mn_{12}O_{24}$ and $Mn_{16}O_{32}$ surfaces with the bottom Mn_4O_8 fixed could get reasonable structures. We used the $Mn_{12}O_{24}$ model, as shown in Fig. 2, in the later calculations because of shorter calculation time needed.

3.2.2. α-MnO_2 (1 1 0) surfaces with different kinds of terminations and magnetic arrangements

We focused on the different kinds of surface terminations and magnetic arrangements based on the $Mn_{12}O_{24}$ model and fixed the bottom Mn_4O_8 atoms. The perpendicular separation between the slabs was about 30 Å, which guaranteed no interaction between the slabs. The Monkhorst–Pack k point sampling was set as $5 \times 2 \times 1$ in the supercell [23]. To build all the possible surface terminations, we began with the T1 structure in Fig. 2A, then moved the bottom Mn atom to the surface top to build the next termination T2 in Fig. 2B. It seems that we have considered all the possible surface structures, because Yamamoto et al. found that there was no reconstruction on the (1 1 0) surface of powdered α-MnO_2 [8]. Fig. 2 shows the optimized surface terminations T1–T10. In Fig. 2, T1, T2, T4, T8 and T9 maintained the surface structures from crystal, but there were reconstructions for T3, T5, T6, T7 and T10. For each surfaces in Fig. 2, different kinds of magnetic arrangement such as NM, FM and some AFM states were simulated. With the same trend of crystal, the NM and FM states were less favorable than the AFM states. For example, the NM and FM surface energies of T1 are 0.54 and 0.10 J m^{-2} higher than its AFM state. For abbreviation, Fig. 2 only shows the low energy AFM structures. Table 2 lists their surface energies. Judging from the surface energies of T1 to T10, T1 is the most favorable termination with the lowest surface energy of 0.77 J m^{-2}. The detailed calculated coordinates of T1 are listed in the Supporting materials. It shows that the surface energies of T1 are 0.762 J m^{-2}, 0.743 J m^{-2}, 0.766 J m^{-2} and 0.780 J m^{-2} respectively when the global orbital cutoffs 4.0 Å, 4.4 Å, 4.7 Å and 5.0 Å are used. Therefore the global orbital cutoff 4.7 Å used in the present paper is suit for calculating the α-MnO_2 (1 1 0) surface.

3.2.3. Large α-MnO_2 (1 1 0) surfaces

We extended the surfaces T1 and T2 four times larger with the supercell $Mn_{48}O_{96}$ to make a further test of surface energy and magnetic arrangement. The Monkhorst–Pack k point sampling was set as $6 \times 2 \times 1$ in the supercell [23]. Table 3 lists three kinds of magnetic arrangements for T1 and T2. It is clear that these magnetic arrangements have similar surface energies. On the other hand, the larger surface area has little influence on the surface energy. The surface energies of T1 and T2 in Tables 2 and 3 are almost the same. From Fig. 3A–C, we can see that the most stable surface T1 exposes the crystal 2×2 semitunnel to air and the crystal 1×1 tunnel does not expose. The surface Mn cations move outside the surface when there are O atoms on the surface such as in T2, but they move inside without O atoms such as in T1.The detailed calculated coordinates of T1 and T2 are listed in the Supporting materials.

The oxygen-lean and oxygen-rich α-MnO_2 surfaces used by Tang et al. [15,16] are similar to T1 and T2 in this paper, while they did not mention the magnetic arrangement. It is easy to see that T1 would become T2 when another O atom comes to the surface, but the real reaction process maybe complicated and further work is needed.

3.3. The hydroxyl α-MnO_2 (1 1 0) surface

Yamamoto et al. have observed the atomic configuration and topography of the α-MnO_2 surface by atomic force microscopy [8]. They found that there is no reconstruction on the hydroxyl

Table 2
Surface energies γ (J m^{-2}) of different kinds of stable surface terminations with the favorite AFM state.

	T1	T2	T3	T4	T5	T6	T7	T8	T9	T10
γ (J m^{-2})	0.77	2.86	2.15	1.28	4.78	6.05	4.83	1.27	3.33	2.69

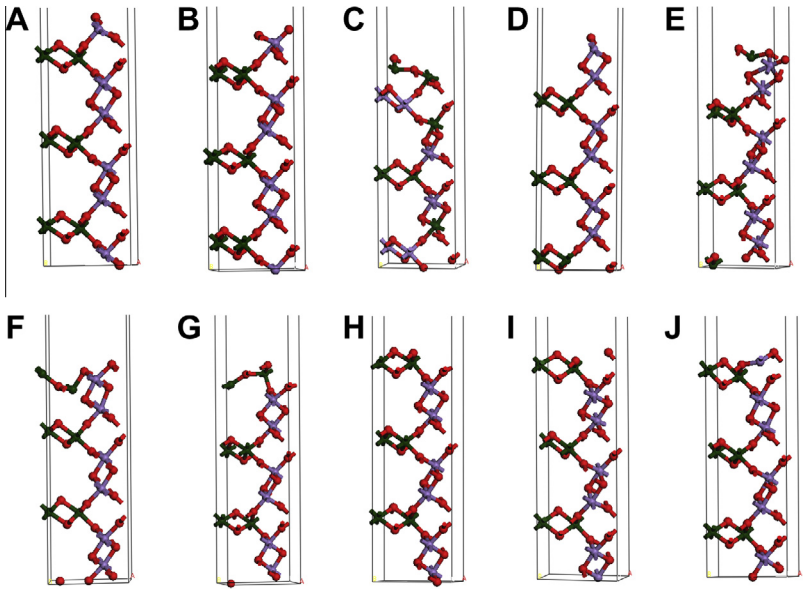

Fig. 2. The optimized α-MnO_2 (1 1 0) surfaces with different kinds of terminations and magnetic arrangements with the supercell $Mn_{12}O_{24}$. (A) T1; (B) T2; (C) T3; (D) T4; (E) T5; (F) T6; (G) T7; (H) T8; (I) T9; and (J) T10.

Table 3
Surface energies γ (J m^{-2}) of T1 and T2 with different kinds of AFM states.

	T1			T2		
	AFM1	AFM2	AFM3	AFM1	AFM2	AFM3
γ (J m^{-2})	0.79	0.78	0.80	2.87	2.87	2.87

(1 1 0) surface because the surface can superimpose on the bulk structure. We put OH^- ions onto the most stable α-MnO_2 surface T1 as shown in Fig. 4, where the H^+ cations are shown with small white ball. The Monkhorst–Pack *k* point sampling was set as $3 \times 1 \times 1$ in the supercell [23]. The comparison of the surface structures with bulk crystal structures is shown in Table 4. From Table 4, we can see that the distances between surface hydroxyl groups are 2.8816 Å (O1–O11) and 7.1254 Å (O1–O22), which are only 0.04% and 0.33% larger than the corresponding distances between O ions in the bulk crystal. When we compare these distances with the atomic force microscopy results [8], the experimental result 2.6 Å for O1–O11 is a little smaller than our theoretical result 2.8816 Å, while the experimental result 8 Å for O1–O22 is larger than our theoretical result 7.1254 Å. From Fig. 4 and Table

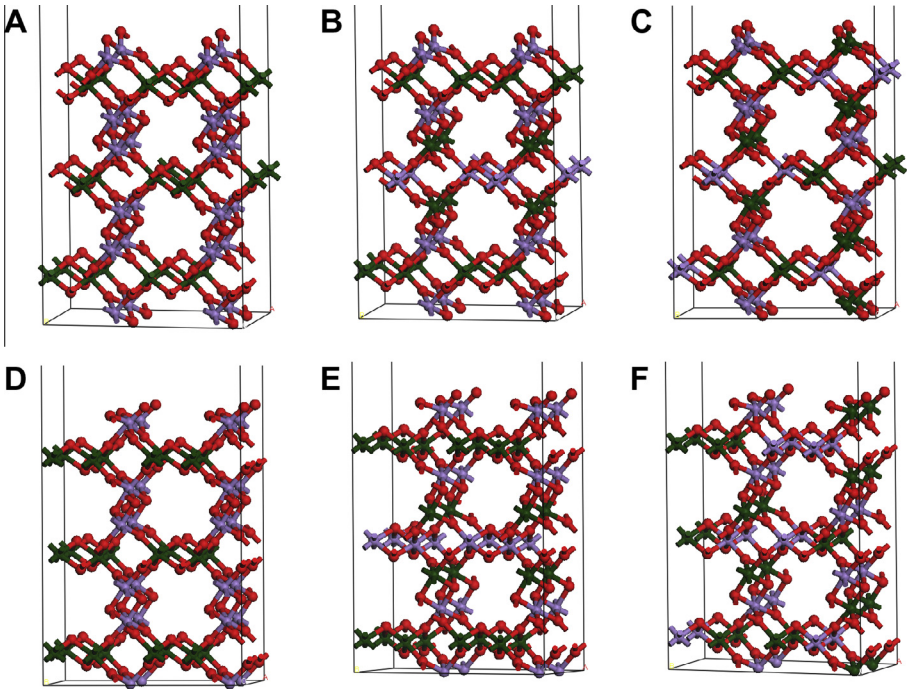

Fig. 3. The optimized α-MnO_2 (1 1 0) surfaces T1 and T2 with the supercell $Mn_{48}O_{96}$. (A) AFM1 state of T1; (B) AFM2 state of T1; (C) AFM3 state of T1; (D) AFM1 state of T2; (E) AFM2 state of T2; and (F) AFM3 state of T2.

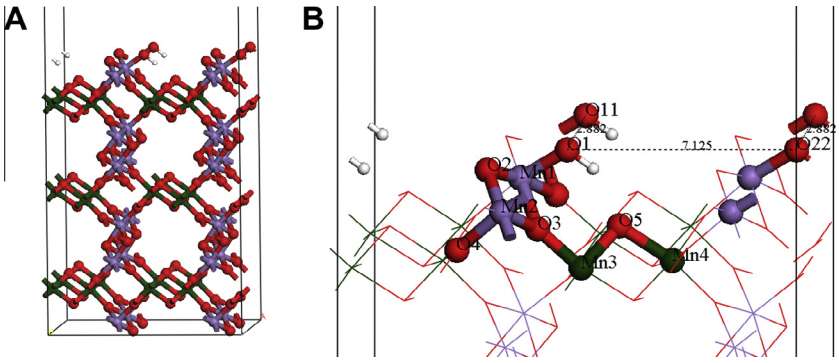

Fig. 4. α-MnO_2 (1 1 0) surface with OH^- ions (the H^+ cations are shown in small white). (A) The whole surface; and (B) the top of the surface.

Table 4
Comparison of the optimized hydroxyl (1 1 0) surface with the corresponding bulk crystal structures (Å) and percent relaxations.

	O1–O11	O1–O22	Mn1–O1	Mn2–O4	Mn2–O2	Mn2–O3	Mn3–O3	Mn3–O5	Mn4–O5
Surface	2.8816	7.1254	1.8272	1.9889	1.8010	1.9949	1.8189	1.9304	1.9709
Crystal	2.8805	7.1019	1.9323	1.8881	1.9137	1.9056	1.8881	1.9137	1.9323
Relaxation	+0.04	+0.33	−5.4	+5.3	−5.9	+4.7	−3.7	+0.9	+2.0

4, we can see that the adsorption of hydroxyl group makes the surface Mn cations such as Mn1 and Mn2 move outside the surface by increase the bond Mn2–O4 longer about 5.3%. It is reasonable that the surface bonds Mn2–O2 and Mn1–O2 would become shorter when there are only two Mn–O bonds for O2, and the surface bonds Mn3–O5 and Mn4–O5 would become longer when O5 exposes to the air. The bond Mn2–O3 extends from 1.9056 Å in the bulk to 1.9949 Å at the surface, while the bond Mn3–O3 shrinks from 1.8881 Å in the bulk to 1.8189 Å at the surface. It is clear that our simulation results are reasonable to the hydroxyl adsorption. The detailed calculated coordinates of the hydroxyl T1 surface are listed in the Supporting materials.

4. Conclusion

First-principles DFT calculations have been used to investigate the α-MnO_2 crystal and its (1 1 0) surface. For the crystal, our results fit well with previous experiments and calculations. In addition, we found a new AFM state for the crystal, which is 3.096 meV per formula lower in energy than that reported by Cockayne and Li [12]. For both crystal and surface, the NM and FM states are less stable than the AFM states, but some AFM states have similar stabilities. We have calculated all the possible no reconstruction terminations to find the most stable AFM α-MnO_2 (1 1 0) surface T1, which exposes the crystal 2×2 semitunnel and possesses the lowest surface energy of 0.77 J m^{-2}. The hydroxyl α-MnO_2 (1 1 0) surface is also simulated with reasonable changes from the crystal structure. Therefore, these results provide some basic information to understand the α-MnO_2 crystal and its (1 1 0) surface.

Acknowledgements

This work was supported by Natural Science Foundation of Guangdong Province (10251009001000003), National Natural Science Foundation of China (20803014) and the 211 Project of Guangdong Province.

Appendix A. Supplementary material

Supplementary material associated with this article can be found, in the online version, at http://dx.doi.org/10.1016/j.comptc.2014.01.003.

References

[1] V.B.R. Boppana, F. Jiao, Nanostructured MnO_2: an efficient and robust water oxidation catalyst, Chem. Commun. 47 (2011) 8973–8975.
[2] R.S. Kalubarme, M.S. Cho, K.S. Yun, T.S. Kim, C.J. Park, Catalytic characteristics of MnO_2 nanostructures for the O_2 reduction process, Nanotechnology 22 (2011) 395402.
[3] M. Sun, B. Lan, L. Yu, F. Ye, W. Song, J. He, G.Q. Diao, Y.Y. Zheng, Manganese oxides with different crystalline structures: facile hydrothermal synthesis and catalytic activities, Mater. Lett. 86 (2012) 18–20.
[4] T. Gao, M. Glerup, F. Krumeich, R. Nesper, H. Fjellvag, P. Norby, Microstructures and spectroscopic properties of cryptomelane-type manganese dioxide nanofibers, J. Phys. Chem. C 112 (2008) 13134–13140.
[5] L. Espinal, W. Wong-Ng, J.A. Kaduk, A.J. Allen, C.R. Snyder, C. Chiu, D.W. Siderius, L. Li, E. Cockayne, A.E. Espinal, S.L. Suib, Time-dependent CO_2 sorption hysteresis in a one-dimensional microporous octahedral molecular sieve, J. Am. Chem. Soc. 134 (2012) 7944–7951.
[6] H. Sato, T. Enoki, J.I. Yamaura, N. Yamamoto, Charge localization and successive magnetic phase transitions of mixed-valence manganese oxides $K_{1.5}(H_3O)_xMn_8O_{16}$ ($0 < x < 0.5$), Phys. Rev. B 59 (1999) 12836–12841.
[7] J. Luo, H.T. Zhu, J.K. Liang, G.H. Rao, J.B. Li, Z.M. Du, Tuning magnetic properties of α-MnO_2 nanotubes by K^+ doping, J. Phys. Chem. C 114 (2010) 8782–8786.
[8] O.M.S. Yamamoto, I. Fukada, Y. Ashida, T. Honda, N. Yamamotoy, Using atomic force microscopy to image the surface of the powdered catalyst KMn_8O_{16}, J. Catal. 159 (1996) 401–409.
[9] C. Franchini, R. Podloucky, J. Paier, M. Marsman, G. Kresse, Ground-state properties of multivalent manganese oxides: density functional and hybrid density functional calculations, Phys. Rev. B 75 (2007) 195128.
[10] K.D. Kwon, K. Refson, G. Sposito, Defect-induced photoconductivity in layered manganese oxides: a density functional theory study, Phys. Rev. Lett. 100 (2008) 146601.
[11] G.A.E. Oxford, A.M. Chaka, Oxidized, and reduced β-MnO_2 surfaces, J. Phys. Chem. C 115 (2011) 16992–17008.
[12] E. Cockayne, L. Li, First-principles DFT + U studies of the atomic, electronic, and magnetic structure of α-MnO_2 (cryptomelane), Chem. Phys. Lett. 544 (2012) 53–58.
[13] Y.P. Duan, Z. Liu, Y.H. Zhang, M. Wen, A theoretical study of the dielectric and magnetic responses of Fe-doped α-MnO2 based on quantum mechanical calculations, J. Mater. Chem. C 1 (2013) 1990–1994.
[14] Y.P. Duan, Z. Liu, H. Jing, Y.H. Zhang, S.Q. Li, Novel microwave dielectric response of Ni/Co-doped manganese dioxides and their microwave absorbing properties, J. Mater. Chem. 22 (2012) 18291–18299.

[15] C. Wang, L. Sun, Q.Q. Cao, B.Q. Hu, Z.W. Huang, X.F. Tang, Surface structure sensitivity of manganese oxides for low-temperature selective catalytic reduction of NO with NH_3, Appl. Catal. B: Environ. 101 (2011) 598–605.
[16] P.P. Hu, Z.W. Huang, W.M. Hua, X. Gu, X.F. Tang, Effect of H_2O on catalytic performance of manganese oxides in NO reduction by NH_3, App. Catal. A: General 437–438 (2012) 139–148.
[17] J.P. Perdew, Y. Wang, Accurate and simple analytic representation of the electron-gas correlation energy, Phys. Rev. B. 45 (1992) 13244–13249.
[18] N.A. Benedek, I.K. Snook, K. Latham, I. Yarovsky, Application of numerical basis sets to hydrogen bonded systems: a density functional theory study, J. Chem. Phys. 122 (2005) 144102.
[19] A.I. Liechtenstein, V.I. Anisimov, J. Zaanen, Density-functional theory and strong-interactions – orbital ordering in Mott-Hubbard insulators, Phys. Rev. B 52 (1995) R5467–R5470.
[20] B. Delley, An all-electron numerical method for solving the local density functional for polyatomic molecules, J. Chem. Phys. 92 (1990) 508–517.
[21] B. Delley, Fast calculation of electrostatics in crystals and large molecules, J. Chem. Phys. 100 (1996) 6107–6110.
[22] B. Delley, From molecules to solids with the DMol(3) approach, J. Chem. Phys. 113 (2000) 7756–7764.
[23] H.J. Monkhorst, J.D. Pack, Special points for brillouin-zone integrations, Phys. Rev. B 13 (1976) 5188–5192.